nature communications

Article

https://doi.org/10.1038/s41467-025-56312-z

# High-temperature structural disorders stabilize hydrous aluminosilicates in the mantle transition zone

Received: 26 March 2024

Accepted: 15 January 2025

Published online: 26 January 2025

Check for updates

Baoyun Wang[1], Jin Liu[2] ✉, Yanyao Zhang[3], Baisheng Nie[4], Wei Yang[5], Jialong Hao[5], Xing Ding[6] & Yongjun Tian[2]

Hydrous aluminosilicates are important deep water-carriers in sediments subducting into the deep mantle. To date, it remains enigmatic how hydrous aluminosilicates withstand extremely high temperatures in the mantle transition zone. Here we systematically investigate the crystal structures and chemical compositions of typical hydrous aluminosilicates using single-crystal X-ray diffraction, electron probe microanalyzer, and nanoscale secondary ion mass spectrometry. These single crystals are synthesized at 15.5–22.0 GPa and 1400–1700 °C, featuring pervasive structural disorders. In particular, Al and Si atoms extensively occupy new tetrahedral and octahedral sites that are nominally vacant in their ordered counterparts. High temperature activates disorders leading to variable local crystal structures and more hydrogen incorporation into the crystal structure. This result suggests that the order-to-disorder transition holds the key to the high thermal stability of hydrous aluminosilicates, significantly affecting the water cycle in the deep mantle.

Geophysical observations, high pressure-temperature (*P-T*) experiments, and natural samples from the deep mantle indicate the existence of water within the Earth[1–7]. Hydrous minerals and nominally anhydrous minerals (NAMs) have been considered potential carriers of surface water into the Earth's interior via subducting slabs[8,9]. Recently, high *P-T* experiments suggest that some hydrous minerals in hydrated subducting slabs may transport water to the core-mantle boundary[10–12]. The release of water from dehydration of those minerals can influence mantle viscosity, conductivity, and phase relations, as well as magma and earthquake generation in the Earth's interior[11–15]. Notably, major mantle minerals exhibit limited water solubility[16–18]. Therefore, if high-pressure hydrous minerals can withstand high temperatures in the mantle, the water reservoirs and fluxes may be significant in the Earth's deep interior.

The Earth's mantle transition zone (MTZ) is considered to be the primary water reservoir in the deep mantle, playing an essential role in mantle structure and dynamics[19–24]. Dense hydrous magnesium silicates (DHMS) in hydrated peridotite and hydrous aluminosilicates in hydrated sediments may be important water carriers in the MTZ[11]. Unlike DHMS that can be stable only along the cold subduction geotherm, hydrous aluminosilicates generally exhibit remarkably high thermal stability above the normal mantle geotherm in the MTZ, including Topaz-OH I and II ($Al_2SiO_6H_2$), phase Psi ($Al_2SiO_6H_2$), the Al endmember of phase D ($Al_2SiO_6H_2$), phase Egg ($AlSiO_4H$) and two unknown phases[25–31]. Notably, the Al endmember of phase D, phase Egg, and two unknown phases can remain stable up to 2000 °C under MTZ pressures[27,31]. Therefore, these hydrous aluminosilicates may play a crucial role in the water storage and cycle in high-temperature,

[1]School of Earth Sciences, Lanzhou University, Lanzhou 730000, China. [2]Center for High Pressure Science, State Key Laboratory of Metastable Materials Science and Technology, Yanshan University, Qinhuangdao 066004, China. [3]Earth and Planetary Sciences, Stanford University, Stanford, CA 94305, USA. [4]State Key Laboratory of Coal Mine Disaster Dynamics and Control, School of Resources and Safety Engineering, Chongqing University, Chongqing 400044, China. [5]Key Laboratory of Earth and Planetary Physics, Institute of Geology and Geophysics, Chinese Academy of Sciences, Beijing 100029, China. [6]State Key Laboratory of Isotope Geochemistry, Guangzhou Institute of Geochemistry, Chinese Academy of Sciences, Guangzhou 510000, China.
✉e-mail: jinliu@ysu.edu.cn

localized water-rich regions of the MTZ. However, the structural mechanism behind their high thermal stability remains unclear.

In this study, we systematically characterized typical hydrous aluminosilicates including Topaz-OH I, Topaz-OH II, phase Egg, and phase Psi, synthesized under normal mantle geotherm conditions in the MTZ, using single-crystal X-ray diffraction (XRD), electron probe microanalyzer (EPMA), nanoscale secondary ion mass spectrometry (NanoSIMS) and Raman spectroscopy. The high *P-T* experimental conditions and results are provided in Supplementary Tables 1–2. High-quality crystal structure data allowed us to comprehensively elucidate the evolution of crystal structures of hydrous aluminosilicates with increasing temperature under MTZ pressures. Particularly, we observed pervasive structural disorders in these phases under high temperatures. This result provides a universal perspective for understanding the unusual thermal stability of hydrous aluminosilicates, paving the way for the exploration of new stable hydrous phases in the deep mantle.

## Results and Discussion

### Structural disorders in hydrous aluminosilicates

The Si/Al mole ratios range from 0.33 to 0.45 for these synthesized single crystals of Topaz-OH I, Topaz-OH II, and phase Psi (Fig. 1). It is lower than the ideal end-member $Al_2SiO_6H_2$ with a Si/Al mole ratio of 0.5. Further, the Si/Al mole ratios of phase Egg fall between 0.52 and 0.58, which are also lower than the ideal end-member $AlSiO_4H$ with a Si/Al mole ratio of 1.0. These deviations from the ideal chemical formulae indicate the presence of structural disorders in their crystals. Our single-crystal XRD results are in support of this speculation (Supplementary Notes 1–5). The Al endmember of phase D can be considered a completely disordered phase Psi according to the single-crystal XRD results. In other words, the phase transition from phase Psi to the Al endmember of phase D is isochemical and characterized by disordering of cation distribution among structural sites (see Supplementary Note 3 for more details). Additionally, the previous unknown phases I and II that were first synthesized at 22 GPa and 1527–2002 °C by Takaichi et al.[31], can be identified as disordered phase Egg and phase Psi, respectively (Supplementary Note 5). Besides sharing very similar chemical compositions and Raman spectra, the molded reflection tables using our crystal structure also exhibit high consistency with Takaichi et al.'s powder XRD experimental results[31]. By comparing the crystal structures of synthesized samples under different *P-T* conditions, it is evident that these hydrous phases synthesized under relatively low *P-T* conditions (e.g., cold subduction geotherms) have ordered crystal structures (Fig. 2). For example, in the crystal structures of Topaz-OH I and phase Egg synthesized at 1000 °C, Al and Si

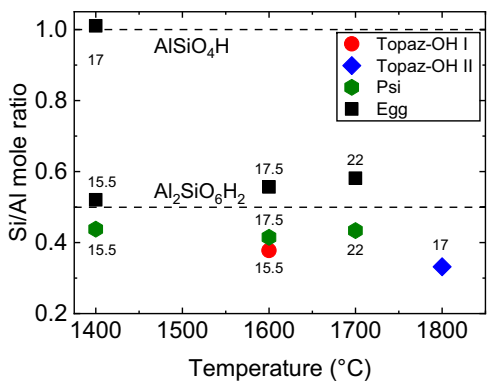


**Fig. 1 | The relations between the Si/Al mole ratio of hydrous aluminosilicate and the synthesis temperature.** $AlSiO_4H$ represents the ideal chemical composition of phase Egg. $Al_2SiO_6H_2$ represents the ideal chemical composition of Topaz-OH I, Topaz-OH II, and phase Psi. Digits denote the synthesis pressure in the unit of GPa.

consistently occupy their respective structural sites without any apparent positional and substitutional disorder[32,33]. However, with increasing the synthesis temperatures, these synthesized at higher *P-T* conditions may exhibit disordered crystal structures. They exhibit varying temperatures for the transitions from ordered to disordered states, which seemingly increase gradually with pressure. In general, these hydrous phases synthesized under the normal mantle geotherm display disordered structures (Fig. 2).

All these disordered hydrous phases show partial occupancy at certain structural sites in the corresponding ordered structures based on our crystal structure analyses (Supplementary Notes 1–5). For instance, the occupancy of the normal aluminum octahedral Al1 site is only 0.899 in disordered Topaz-OH I (Fig. 3). Interestingly, new structural sites are found in their crystal structures, which are completely vacant in the ordered counterpart. Notably, in disordered Topaz-OH I, a new octahedral Al2 site is coplanar with the tetrahedral Si1 site (Fig. 3a, b). As the degree of disorder enhanced by high temperatures, Al and Si would randomly occupy the three octahedral and tetrahedral sites along the *c*-axis, leading to the phase transition from ordered Topaz-OH I to partially disordered Topaz-OH I and completely disordered Topaz-OH II. The three phases belong to the same space group *Pbnm*, with the similar *a* and *b* values, but the *c* value in Topaz-OH II is only 1/3 of that in ordered Topaz-OH I (Fig. 3c and Supplementary Notes 1–2). Similarly, partial Al and Si atoms would occupy the normally vacant octahedral sites in hydrous phase Psi as the degree of structural disorder gradually increases under *P-T* conditions. This leads to the phase transition to the fully disordered Al endmember of phase D (Supplementary Note 3). Due to the comparable scattering factors of Al and Si atoms and the limited knowledge on the impact of vacancies on polyhedral bond lengths, a quantitative study of the Al/Si ratio at each structural site after structural disorder remains challenging. Alternatively, by combining EPMA results, we find that in disordered Topaz-OH II and disordered phase Egg, Al and Si atoms would jointly occupy certain structural sites, indicating substitution disorder (Fig. 3). In particular, for the disordered phase Egg sample synthesized at 22 GPa and 1700 °C, crystal structure refinements reveal that the total occupancy of the octahedral Si1 sites is 0.938, while the chemical formula for Si from EPMA is only 0.68 (Supplementary Note 4). This indicates the presence of Al in the octahedral Si1 sites.

### Structural disorders affect hydrogen incorporation

Hydrous aluminosilicates exhibit extensive crystal structure disorders under high *P-T* conditions, resulting in diverse local environments. This provides potential sites for hydrogen (H) incorporation to balance the bonding valence of oxygen atoms. Based on the incorporation of H into defects in hydrous minerals or NAMs[34–36], we propose the following three main possible substitution mechanisms for these hydrous aluminosilicates in the MTZ:

$$Si^{4+} \rightarrow \text{vacancy} + 4H^{+} \quad (1)$$

$$Al^{3+} \rightarrow \text{vacancy} + 3H^{+} \quad (2)$$

$$Si^{4+} \rightarrow Al^{3+} + H^{+} \quad (3)$$

The crystal structure analysis indicates that in phase Egg, phase Psi, Topaz-OH I, and Topaz-OH II phases, there are partial occupancies (vacancies) of Al and Si at certain structural sites for H probably entering the crystal by the mechanisms (1) and (2). Besides, Topaz-OH I and phase Egg may hold an extra portion of H through the substitution mechanism (3). In the phase Egg sample, $Al^{3+} + H^{+}$ occupy the octahedral Si1 site. Notably, $Al^{3+} + H^{+}$ does not directly occupy the tetrahedral Si1 site in Topaz-OH I, but rather a new octahedral Al2 site. It is expected that these substitutions increase the water content in the

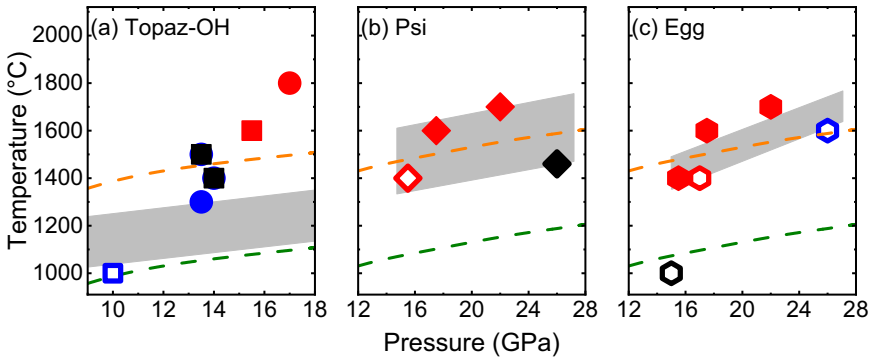


**Fig. 2 | The crystal structure evolution of hydrous aluminosilicates under mantle transition zone conditions.** (**a**) Topaz-OH, (**b**) phase Psi, and (**c**) phase Egg. The solid symbols represent disordered crystal structures, while the open symbols represent ordered crystal structures. Blue square: Topaz-OH I, Wunder et al.[32]; Black square: Topaz-OH I, Xue et al.[25]; Blue circle: Topaz-OH II, Xue et al.[25]; Black diamond: the Al endmember of phase D, Pamato et al.[27]; Black hexagon: phase Egg, Schmidt et al.[33]; Blue hexagon: phase Egg, Schulze et al.[67]; Red symbols: this study. The shaded regions indicate the order-to-disorder transition boundaries. The orange and olivine curves represent normal mantle and cold slab geotherms, respectively[68].

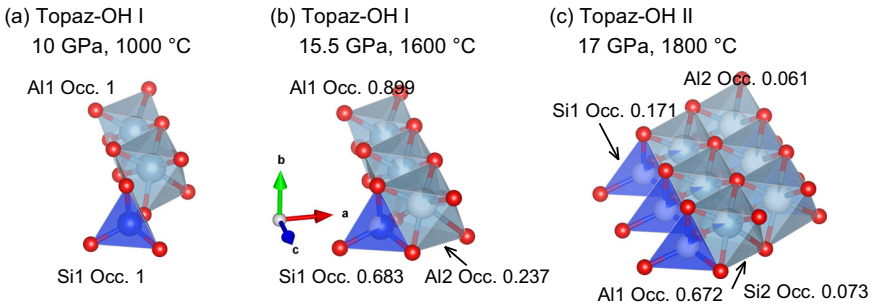


**Fig. 3 | Representative structural disorder mechanisms in typical hydrous aluminosilicates. a** Ordered Topaz-OH I synthesized at 10.0 GPa and 1000 °C by Wunder et al.[32]. **b** Disordered Topaz-OH I and **c** Disordered Topaz-OH II synthesized at 15.5 GPa and 17.0 GPa, respectively, in this study. The *c*-axis of Topaz-OH II is enlarged three times for better comparison.

crystals, as indicated by EPMA and NanoSIMS measurements, showing that the disordered phase has higher water content than the ordered counterpart (Supplementary Tables 1–2). The elevated water contents during high-temperature induced order-disorder transitions in hydrous aluminosilicates differ from most of other mantle minerals because water content typically decreases in other water-bearing phases at elevated temperatures[19,20]. These hydrous aluminosilicates feature Raman peaks associated with hydroxyl stretching vibrations in the range of 2000–4000 $cm^{-1}$ (Supplementary Figs. 6–8). In comparison to the ordered phase Egg and phase Psi synthesized at relatively low *P-T* conditions, new Raman bands emerge at around 3150 $cm^{-1}$ for the disordered phase Egg and phase Psi. Additionally, the Raman peaks in Topaz-OH II are noticeably broader, consistent with its higher degree of structural disorders, with respect to Topaz-OH I.

## Structural disorders enhance thermal stability

Further, the octahedral layers of these hydrous aluminosilicates feature a thickness of around 4.3 Å. The distinct layers are formed by the hexagonal close-packing of oxygen atoms according to our single-crystal structural analyses on these hydrous aluminosilicates (Supplementary Tables 4–15). Under high *P-T* conditions of the MTZ, both Al and Si atoms could adopt octahedral coordination, allowing them to co-occupy the same octahedral site. Meanwhile, Al and Si atoms may randomly occupy or diffuse into new octahedral sites due to the similar energy of different sites during crystal growth at high temperatures. Therefore, structural disorders are likely to be widespread in these phases. These local structures are governed by some basic rules, including the exclusion of atoms simultaneously occupying two co-planar octahedra, valence balance, and the minimization of the thermodynamic energy of the system[25,37]. In general, structural disorders can broaden the phase stability field of minerals by increasing configurational entropy[38–40]. For example, in some hydrous minerals like brucite and phase X and NAMs such as ringwoodite, a certain degree of structural disorder is favored under high *P-T* conditions[41–44]. Notably, the Mg endmember of DHMS can only withstand the cold subduction geotherm; Al-bearing DHMS, however, can remain stable along the warm subduction geotherm, even along the normal mantle geotherm because of cation mixing at octahedral sites[45–48]. Given that typical hydrous aluminosilicates exhibit remarkable thermal stability up to 2000 °C, it is conceivable that structural disorders play a significant role in deep water cycling in the MTZ and the lower mantle.

## Hydrous aluminosilicates contribute to the deep-water cycle

The stable hydrous aluminosilicates evolve with increasing depth in the MTZ as shown in Supplementary Fig. 9. Topaz-OH I and Topaz-OH II are suggested to be stable in the upper part of the MTZ, while phase Egg, phase Psi, and the Al endmember of phase D are stable in the lower part of the MTZ. Phase Egg remains stable at least up to 30 GPa[30]. Thus far, the phase diagrams of phase Egg and the Al endmember of phase D under lower mantle conditions have not been well constrained. In addition, δ-AlOOH remains stable along cold slab geotherms to the core-mantle boundary[49]. Further studies are needed to determine their complete phase stability fields and evaluate the maximum depth of the water cycle involving hydrous aluminosilicates.

Subducting slabs consist primarily of harzburgite, oceanic crust, and overlying sediments. It is widely recognized that significant

amounts of water can be transported into the Earth's interior by hydrous minerals within the slab[12]. In principle, the depth of this water transport is closely linked to the thermal stability of hydrous minerals and the thermal structure of the slab. The primary hydrous minerals in hydrated oceanic crusts and hydrated peridotites, such as lawsonite, serpentine, and DHMS phases, can only remain stable under cold subduction thermal gradients[11]. Consequently, they are likely to decompose at relatively shallow depths in warm-hot subduction zones, where higher thermal gradients make it improbable for them to carry water into the deep mantle. We propose that hydrous aluminosilicates with ultra-high thermal stability within the sediment layer of the subducting slab may serve as the primary water carriers in those warm-hot subduction zones. This sediment layer can form hydrous aluminosilicates through the reaction between aluminum-rich materials and water at high *P-T* during subduction. Meanwhile, water generated from the thermal decomposition of hydrous minerals in both hydrous oceanic crusts and mantle rocks may not fully escape to the surrounding mantle but rather be captured by the sediment layer. The formation of hydrous aluminosilicates can transport water deeper into the Earth. Based on the high *P-T* phase diagrams of hydrous aluminosilicates and sediments[27,29,30,50,51] (Supplementary Fig. 9), it is evident that these minerals may carry water into the MTZ and the lower mantle as the subducting slab descends. Our results indicate that these hydrous aluminosilicates modify their crystal structures through disordering to better adapt to high *T* environments. Sediment layers lie atop the subducting slab; during slow subduction, *T* gradually aligns with the high *T* profile of the overlying mantle. Consequently, hydrous aluminosilicates in hydrated sediments are prone to have disordered structures. In certain cold subduction zones, such as Tonga, the ordered phases such as Topaz-OH I and phase Egg may form at shallower depths, while the disordered phase Egg, phase Psi, and the Al endmember of phase D form at greater depths[52] (Fig. 4).

The MTZ is believed to be at least locally water-rich, as indicated by the high water solubility of wadsleyite and ringwoodite, along with geophysical observations and natural diamond inclusions[1,4,7,19–22,53]. Previous experiments show that wadsleyite and ringwoodite can accommodate approximately 1 wt.% water under normal mantle thermal gradients in the MTZ and their water solubility gradually decreases with increasing temperature[19,20,54]. The partition coefficient of water between olivine polymorphs (e.g., wadsleyite and ringwoodite) and hydrous aluminosilicates remain unconstrained by experiments. On the other hand, considering the heterogeneous distribution of water in the MTZ and the capability of hydrous aluminosilicates to retain largely about 10 wt.% water up to 2000 °C, these hydrous aluminosilicates likely play a significant role in water storage locally in the MTZ. Hydrous aluminosilicates even may absorb water released by wadsleyite and ringwoodite with increasing *T*. This can assist in the transport of water down to the lower mantle via subducting slabs. Given that the primary lower-mantle minerals, bridgmanite, and ferropericlase, can only contain up to 2000 ppm of water, the presence of these hydrous aluminosilicates would significantly influence the local water content in the lower mantle[17,55,56]. Notably, Wirth et al.[53] suggested that phase Egg occurs as inclusions in ultra-deep diamonds, providing strong support for the existence of hydrous aluminosilicates in the Earth's interior.

Subducted sediments are probably to sponge up surrounding water to form hydrous aluminosilicates, even under normal mantle geotherms[25,28,29,50]. Hydrous sediments could accumulate in the MTZ due to slab stagnation and/or at the top of the lower mantle through slab penetration. Consequently, this is likely to create water-rich domains/patches in the deep mantle, which may persist for protracted periods in geological history due to the extremely high thermal stability of hydrous aluminosilicates. When those sediments release water due to thermal decomposition in the lower mantle, significant changes can occur in the physical and chemical properties of surrounding mantle, potentially leading to magma generation and mantle plumes[11,50]. Meanwhile, disordered hydrous aluminosilicates may form from hydrated melts interacting with sediments, which could ascend along with upwell plume and then undergo dehydration in the shallow upper mantle (Fig. 4). One prediction of this model is that the magma carrying those materials would be enriched in water and retain the geochemical signatures of subducted sediments, aligning with field observations from certain ocean island basalts[57–60]. As depicted in Fig. 4, hydrous sediments in subducting slabs establish a complete deep-water cycle, transporting water from the Earth's surface to the MTZ or the top of the lower mantle, and then returning it to the surface via ascending magma from these regions. This implies that water in ocean island basalts may entirely result from the recycling of hydrated slabs, without the need to hypothesize a primordial source. This prediction is supported by recent potassium isotope studies, which proposed that the water associated with Cenozoic volcanic rocks in Northeast Asia has been recycled from the Earth's surface by subduction-related processes, rather than originating from primordial sources[61].

## Methods

### Sample preparation

High-quality single crystals of Topaz-OH I, Topaz-OH II, phase Egg, phase Psi were synthesized under high *P-T* conditions using the Sakura 2500-ton multi-anvil apparatus at the Guangzhou Institute of Geochemistry, Chinese Academy of Sciences. A mixture of $CaCO_3$, $Al(OH)_3$, and $SiO_2$ with a mole ratio of 1:4:2 (mixture 1) or $Al(OH)_3$ and $SiO_2$ in a 2:1 mole ratio (mixture 2) was used as the starting material, sealed in welded gold or platinum capsules. The experiments were conducted using 14/8 or 10/5 octahedral sample assemblies (Cr-doped MgO octahedral edge length / tungsten carbide cubes truncation edge length). The high temperature was generated using a $LaCrO_3$ furnace, and temperature measurement was performed using $W_{95}Re_5$-$W_{74}Re_{26}$ thermocouples. In each run, the sample was initially compressed to the target pressure at room temperature and then heated to the target temperature at a heating rate of approximately 33.3 K/minute. After maintaining the sample at the target temperature for a specific duration, the power was switched off to rapidly cool the sample to room temperature. More detailed information regarding sample assembly, pressure calibration, and experimental procedures can be found in the previous literature[62]. In some runs, several coexisting phases were obtained, while in some cases, a single phase was obtained. The phases were primarily determined by Raman spectroscopy, EPMA, and single-crystal XRD (Supplementary Tables 1–2). The partial experimental results can be also found in a separate paper[26].

### Chemical analysis by electron probe microanalyzer

The recovered capsules were cut into two parts by knives or diamond saws. All products comprised large, transparent, and colorless single crystals as well as small powders. For each experimental run, several randomly chosen crystal grains were polished to determine their chemical compositions. Analysis was conducted using a JEOL JXA-iSP100 electron probe microanalyzer (EPMA) with an accelerating voltage of 15 kV, a beam current of 5 nA, and a beam spot size of approximately 2 μm. Calibration standards of garnet and diopside were utilized to quantitatively measure the Al and Si contents, respectively. Each grain was measured at seven different points, and the average value was computed as the chemical composition of the respective grain. The final chemical composition is the average of multiple grains. All weight losses were considered as water, and the chemical formula for each hydrous phase is derived (Supplementary Tables 1–2).

### Water content determined by NanoSIMS

The water contents of the hydrous samples in this study were measured using a CAMECA NanoSIMS 50 L ion microprobe at the Institute

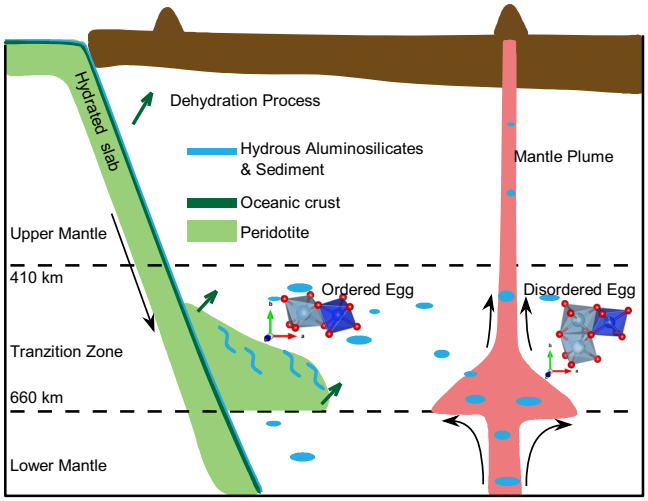


**Fig. 4 | Schematics of the deep water cycle in the presence of hydrous aluminosilicates in the Earth's mantle.** Hydrous minerals in mantle peridotite, oceanic crust, and sediments of subducting slabs, such as hydrous aluminosilicates, can transport water into the deep mantle and recycle it back to the Earth's surface. The crystal structures of hydrous aluminosilicates are significantly influenced by the thermal structure of the deep mantle. Notably, high-temperature induced order-to-disorder transitions of hydrous aluminosilicates potentially result in disordered structures pervasive in slowly hot subducting slabs and mantle plumes (e.g., disordered phase Egg), while ordered structures may dominate in relatively cold subducting slabs (e.g., ordered phase Egg).

of Geology and Geophysics, Chinese Academy of Sciences. Prior to analysis, the polished samples were embedded in indium disks, coated with gold, and mounted on the sample holders alongside standards. The sample holders were then placed into the NanoSIMS chamber under a vacuum of $<3.0 \times 10^{-10}$ torr. NanoSIMS analysis used a $Cs^+$ ion beam with a current of 300 pA, simultaneously collecting secondary anions ($^1H^-$, and $^{18}O^-$) on electron multipliers (EMs) and a Faraday cup detector. To ensure contamination-free analysis, each sample's surface was pre-sputtered for approximately 10 s over a $10 \times 10$ μm area to remove the Au coating, which was monitored in real-time imaging mode. Analyses were conducted on a central $5 \times 5$ μm region using a blanking technique, with each measurement consisting of 200 cycles. A 44 ns dead time correction was applied to all EMs, and an electron gun provided charge compensation. For each measurement, the total counts of $^1H^-$ and $^{18}O^-$ were collected over 200 cycles, allowing for the calculation of the $^1H^-/^{18}O^-$ ratios[63]. These ratios were used to determine the water content based on the phase Egg sample from run # U801 as a reference standard. Additionally, San Carlos olivine was utilized as the background for H intensities. Both EPMA and single-crystal XRD data suggest that the phase Egg sample of U801 is highly ordered, indicating it closely resembles the ideal chemical formula ($AlSiO_4H$) with 7.5 wt.% water. Accordingly, we calculated the water content for each of the hydrous samples in this study (Supplementary Table 1).

### Single-crystal XRD measurements

We selected each hydrous phase under a polarizing microscope for single-crystal XRD experiments, and some crystals are double-sided polished. For single-crystal XRD measurements, a Bruker D8 Venture diffractometer equipped with a *Mo Kα* radiation source (wavelength of 0.71073 Å). The frames were integrated the Bruker SAINT software package, and a multi-scan absorption correction was applied using SADABS[64]. The structure was solved through direct methods using SHELXS or SHELXT and refined using full-matrix least-squares methods against $F^2$ by SHELXL[65,66]. Due to the weak scattering of hydrogen atoms, their positions were not determined. Additionally, the comparable scattering of aluminum and silicon, coupled with the lack of quantitative results on the impact of vacancies on octahedral bond lengths, hindered the differentiation of Al/Si proportions at specific positions. For each hydrous phase, atomic identification was based on occupancy, their ordered crystal structure, and EPMA-derived chemical formulas. During refinement, free variables were introduced for occupancy of each structural site, with constraints applied to maintain the total Al/Si occupancies at each structural site in line with the EPMA chemical formula. Detailed atomic parameters and refinement results are provided in Supplementary Tables 4–17. Additionally, the structures have been deposited at the Cambridge Crystallographic Data Centre (CCDC), with deposition codes 2325388 for Topaz-OH I, 2325389 for Topaz-OH II, 2325430–2325431 and 2328172 for three phase Psi, 2325571–2325573 and 2325566 for four phase Egg.

### Raman spectra

The Raman spectra were acquired using a high-resolution confocal Raman spectrometer, the WITec alpha 300 R (WITec GmbH, Ulm, Germany), equipped with a TEM single-frequency laser ($\lambda = 532$ nm, maximum laser power = 40 mW). The laser light was focused by a 100× oil immersion objective (numerical aperture = 0.9; Carl Zeiss, Germany) onto the sample and detected by the CCD camera (Andor DU401 BV, Belfast, Northern Ireland). The gratings with 300 lines/mm were employed, resulting in a spectral range covering 100–4000 $cm^{-1}$, with a spectral resolution of approximately 2.5 $cm^{-1}$. The results are presented in Supplementary Figs. 6–8.

## Data availability

The essential data supporting the main findings of this study can be found in the manuscript and Supplementary information. All the X-ray crystallographic structures are deposited at the Cambridge Crystallographic Data Centre (CCDC). The source data are also deposited in https://doi.org/10.5281/zenodo.14502371.

## References

1. Schmandt, B., Jacobsen, S. D., Becker, T. W., Liu, Z. & Dueker, K. G. Dehydration melting at the top of the lower mantle. *Science* **344**, 1265–1268 (2014).
2. Han, G. et al. Pervasive low-velocity layer atop the 410-km discontinuity beneath the northwest Pacific subduction zone: Implications for rheology and geodynamics. *Earth Planet. Sci. Lett.* **554**, 116642 (2020).
3. Mazza, S. E. et al. Sampling the volatile-rich transition zone beneath Bermuda. *Nature* **569**, 398–403 (2019).
4. Fei, H. et al. A nearly water-saturated mantle transition zone inferred from mineral viscosity. *Sci. Adv.* **3**, e1603024 (2017).
5. Nishi, M. et al. Stability of hydrous silicate at high pressures and water transport to the deep lower mantle. *Nat. Geosci.* **7**, 224–227 (2014).
6. Hou, M. et al. Superionic iron oxide-hydroxide in Earth's deep mantle. *Nat. Geosci.* **14**, 174–178 (2021).
7. Gu, T. et al. Hydrous peridotitic fragments of Earth's mantle 660 km discontinuity sampled by a diamond. *Nat. Geosci.* **15**, 950–954 (2022).
8. Zheng, Y., Chen, R., Xu, Z. & Zhang, S. The transport of water in subduction zones. *Sci. China Earth Sci.* **59**, 651–682 (2016).
9. Bell, D. R. & Rossman, G. R. Water in Earth's mantle: the role of nominally anhydrous minerals. *Science* **255**, 1391–1397 (1992).
10. Walter, M. Water transport to the core–mantle boundary. *Natl Sci. Rev.* **8**, nwab007 (2021).
11. Ohtani, E. Hydration and dehydration in Earth's interior. *Annu. Rev. Earth Planet. Sci.* **49**, 253–278 (2021).
12. Ohtani, E. The role of water in Earth's mantle. *Natl Sci. Rev.* **7**, 224–232 (2020).

13. Litasov, K. D. & Ohtani, E. Effect of water on the phase relations in Earth's mantle and deep water cycle. *Adv. High-Press. Mineral.* 115–156 (2007).
14. Cooper, G. F. et al. Variable water input controls evolution of the Lesser Antilles volcanic arc. *Nature* **582**, 525–529 (2020).
15. Ishii, T. & Ohtani, E. Dry metastable olivine and slab deformation in a wet subducting slab. *Nat. Geosci.* **14**, 526–530 (2021).
16. Hirschmann, M. M., Aubaud, C. & Withers, A. C. Storage capacity of $H_2O$ in nominally anhydrous minerals in the upper mantle. *Earth Planet. Sci. Lett.* **236**, 167–181 (2005).
17. Liu, Z. et al. Bridgmanite is nearly dry at the top of the lower mantle. *Earth Planet. Sci. Lett.* **570**, 117088 (2021).
18. Ohtani, E. Hydrous minerals and the storage of water in the deep mantle. *Chem. Geol.* **418**, 6–15 (2015).
19. Fei, H. & Katsura, T. Water solubility in Fe-bearing wadsleyite at mantle transition zone temperatures. *Geophys. Res. Lett.* **48**, e2021GL092836 (2021).
20. Fei, H. & Katsura, T. High water solubility of ringwoodite at mantle transition zone temperature. *Earth Planet. Sci. Lett.* **531**, 115987 (2020).
21. Tschauner, O. et al. Ice-VII inclusions in diamonds: evidence for aqueous fluid in Earth's deep mantle. *Science* **359**, 1136–1139 (2018).
22. Pearson, D. et al. Hydrous mantle transition zone indicated by ringwoodite included within diamond. *Nature* **507**, 221–224 (2014).
23. Karato, S.-i, Karki, B. & Park, J. Deep mantle melting, global water circulation and its implications for the stability of the ocean mass. *Prog. Earth Planet. Sci.* **7**, 1–25 (2020).
24. Karato, S.-i Water distribution across the mantle transition zone and its implications for global material circulation. *Earth Planet. Sci. Lett.* **301**, 413–423 (2011).
25. Xue, X., Kanzaki, M. & Fukui, H. Unique crystal chemistry of two polymorphs of topaz-OH: a multi-nuclear NMR and Raman study. *Am. Mineral.* **95**, 1276–1293 (2010).
26. Wang, B. et al. New hydrous phases in the $Al_2O_3$-$SiO_2$-$H_2O$ system under the mantle transition zone conditions. *Sci. China Earth Sci.* **66**, 730–737 (2023).
27. Pamato, M. G. et al. Lower-mantle water reservoir implied by the extreme stability of a hydrous aluminosilicate. *Nat. Geosci.* **8**, 75–79 (2015).
28. Ono, S. High temperature stability limit of phase egg, $AlSiO_3(OH)$. *Contrib. Mineral. Petrol.* **137**, 83–89 (1999).
29. Fukuyama, K., Ohtani, E., Shibazaki, Y., Kagi, H. & Suzuki, A. Stability field of phase Egg, $AlSiO_3OH$ at high pressure and high temperature: possible water reservoir in mantle transition zone. *J. Mineral. Petrol. Sci.* **112**, 31–35 (2017).
30. Abe, R. et al. In situ X-ray diffraction studies of hydrous aluminosilicate at high pressure and temperature. *J. Mineral. Petrol. Sci.* **113**, 106–111 (2018).
31. Takaichi, G. et al. High-temperature phase relations of hydrous aluminosilicates at 22 GPa in the AlOOH-$AlSiO_3OH$ system. *Am. Mineral.* **108**, 826–831 (2023).
32. Wunder, B. et al. Synthesis, stability, and properties of $Al_2SiO_4(OH)_2$: a fully hydrated analogue of topaz. *Am. Mineral.* **78**, 285–297 (1993).
33. Schmidt, M. W., Finger, L. W., Angel, R. J. & Dinnebier, R. E. Synthesis, crystal structure, and phase relations of $AlSiO_3OH$, a high-pressure hydrous phase. *Am. Mineral.* **83**, 881–888 (1998).
34. Xue, X., Kanzaki, M., Turner, D. & Loroch, D. Hydrogen incorporation mechanisms in forsterite: new insights from $^{1}H$ and $^{29}Si$ NMR spectroscopy and first-principles calculation. *Am. Mineral.* **102**, 519–536 (2017).
35. Ishii, T. et al. Superhydrous aluminous silica phases as major water hosts in high-temperature lower mantle. *Proc. Natl Acad. Sci.* **119**, e2211243119 (2022).
36. Li, X. et al. Synthesis, structure, and single-crystal elasticity of Al-bearing superhydrous phase B. *Am. Mineral.* **107**, 885–895 (2022).
37. Kudoh, Y. et al. Phase E: a high pressure hydrous silicate with unique crystal chemistry. *Phys. Chem. Miner.* **19**, 357–360 (1993).
38. Panero, W. R. & Caracas, R. Stability and solid solutions of hydrous alumino-silicates in the Earth's mantle. *Minerals* **10**, 330 (2020).
39. Dutta, R., Tracy, S. J. & Cohen, R. High-pressure order-disorder transition in $Mg_2SiO_4$: implications for super-Earth mineralogy. *Phys. Rev. B* **107**, 184112 (2023).
40. Dutta, R. et al. Ultrahigh-pressure disordered eight-coordinated phase of $Mg_2GeO_4$: analogue for super-Earth mantles. *Proc. Natl Acad. Sci.* **119**, e2114424119 (2022).
41. Mookherjee, M. & Stixrude, L. High-pressure proton disorder in brucite. *Am. Mineral.* **91**, 127–134 (2006).
42. Hermann, A. & Mookherjee, M. High-pressure phase of brucite stable at Earth's mantle transition zone and lower mantle conditions. *Proc. Natl Acad. Sci.* **113**, 13971–13976 (2016).
43. Welch, M., Bindi, L., Petříček, V. & Plášil, J. Vacancy pairing and superstructure in the high-pressure silicate $K_{1.5}Mg_2Si_2O_7H_{0.5}$: a new potential host for potassium in the deep Earth. *Acta Crystallogr. Sect. B Struct. Sci. Cryst. Eng. Mater.* **72**, 822–827 (2016).
44. Panero, W. R. Cation disorder in ringwoodite and its effects on wave speeds in the Earth's transition zone. *J. Geophys. Res. Solid Earth* **113** (2008).
45. Solomatova, N. V., Caracas, R., Bindi, L. & Asimow, P. D. Ab initio study of the structure and relative stability of $MgSiO_4H_2$ polymorphs at high pressures and temperatures. *Am. Mineral.* **107**, 781–789 (2022).
46. Kakizawa, S. et al. Stability of Al-bearing superhydrous phase B at the mantle transition zone and the uppermost lower mantle. *Am. Mineral.* **103**, 1221–1227 (2018).
47. Xu, C., Inoue, T., Kakizawa, S., Noda, M. & Gao, J. Effect of Al on the stability of dense hydrous magnesium silicate phases to the uppermost lower mantle: implications for water transportation into the deep mantle. *Phys. Chem. Miner.* **48**, 1–10 (2021).
48. Li, X., Speziale, S., Koch-Müller, M., Husband, R. J. & Liermann, H. P. Phase stability of Al-bearing dense hydrous magnesium silicates at topmost lower mantle conditions: implication for water transport in the mantle. *Geophys. Res. Lett.* **49**, e2022GL098353 (2022).
49. Duan, Y. et al. Phase stability and thermal equation of state of δ-AlOOH: implication for water transportation to the deep lower mantle. *Earth Planet. Sci. Lett.* **494**, 92–98 (2018).
50. Ono, S. Stability limits of hydrous minerals in sediment and mid-ocean ridge basalt compositions: Implications for water transport in subduction zones. *J. Geophys. Res.-Solid Earth* **103**, 18253–18267 (1998).
51. Kuritani, T., Ohtani, E. & Kimura, J.-I. Intensive hydration of the mantle transition zone beneath China caused by ancient slab stagnation. *Nat. Geosci.* **4**, 713–716 (2011).
52. Wei, S. S., Wiens, D. A., van Keken, P. E. & Cai, C. Slab temperature controls on the Tonga double seismic zone and slab mantle dehydration. *Sci. Adv.* **3**, e1601755 (2017).
53. Wirth, R., Vollmer, C., Brenker, F., Matsyuk, S. & Kaminsky, F. Inclusions of nanocrystalline hydrous aluminium silicate "Phase Egg" in superdeep diamonds from Juina (Mato Grosso State, Brazil). *Earth Planet. Sci. Lett.* **259**, 384–399 (2007).
54. Druzhbin, D., Fei, H. & Katsura, T. Independent hydrogen incorporation in wadsleyite from oxygen fugacity and non-dissociation of $H_2O$ in the reducing mantle transition zone. *Earth Planet. Sci. Lett.* **557**, 116755 (2021).
55. Fu, S. et al. Water concentration in single-crystal (Al,Fe)-bearing Bridgmanite grown from the hydrous melt: Implications for dehydration melting at the topmost lower mantle. *Geophys. Res. Lett.* **46**, 10346–10357 (2019).
56. Litasov, K. The influence of $Al_2O_3$ on the $H_2O$ content in periclase and ferropericlase at 25 GPa. *Russ. Geol. Geophys.* **51**, 644–649 (2010).

57. Manthilake, G. et al. The electrical conductivity of liebermannite: implications for water transport into the Earth's lower mantle. *J. Geophys. Res. Solid Earth* **125**, e2020JB020094 (2020).
58. Dixon, J. E., Leist, L., Langmuir, C. & Schilling, J.-G. Recycled dehydrated lithosphere observed in plume-influenced mid-ocean-ridge basalt. *Nature* **420**, 385–389 (2002).
59. Blichert-Toft, J., Frey, F. & Albarede, F. Hf isotope evidence for pelagic sediments in the source of Hawaiian basalts. *Science* **285**, 879–882 (1999).
60. Jackson, M. G. & Dasgupta, R. Compositions of HIMU, EM1, and EM2 from global trends between radiogenic isotopes and major elements in ocean island basalts. *Earth Planet. Sci. Lett.* **276**, 175–186 (2008).
61. Xing, K.-C. et al. Potassium isotopic evidence for recycling of surface water into the mantle transition zone. *Nat. Geosci.* **17**, 1–7 (2024).
62. Liu, X., Matsukage, K. N., Nishihara, Y., Suzuki, T. & Takahashi, E. Stability of the hydrous phases of Al-rich phase D and Al-rich phase H in deep subducted oceanic crust. *Am. Mineral.* **104**, 64–72 (2019).
63. Hu, S. et al. Measurements of water content and D/H ratio in apatite and silicate glasses using a NanoSIMS 50L. *J. Anal. At. Spectrom.* **30**, 967–978 (2015).
64. Krause, L., Herbst-Irmer, R., Sheldrick, G. M. & Stalke, D. Comparison of silver and molybdenum microfocus X-ray sources for single-crystal structure determination. *J. Appl. Crystallogr.* **48**, 3–10 (2015).
65. Sheldrick, G. M. Crystal structure refinement with SHELXL. *Acta Crystallogr. Sect. C Struct. Chem.* **71**, 3–8 (2015).
66. Sheldrick, G. M. SHELXT-Integrated space-group and crystal-structure determination. *Acta Crystallogr. Sect. A Found. Adv.* **71**, 3–8 (2015).
67. Schulze, K. et al. High-pressure single-crystal structural analysis of $AlSiO_3OH$ phase egg. *Am. Mineral.* **103**, 1975–1980 (2018).
68. Dziewonski, A. M. & Anderson, D. L. Preliminary reference Earth model. *Phys. Earth Planet. Inter.* **25**, 297–356 (1981).


## Acknowledgements

This work is supported by the National Natural Science Foundation of China: 92479212 (J.L.), 52288102 (J.L.), 42302046 (B.W.), and 42462002 (B.W.). This work is also supported by the Science and Technology Foundation of Guizhou Province (QKHJC-ZK [2023] general 462; B.W.), the Strategic Priority Research Program of the Chinese Academy of Sciences (XDB42000000; X.D.), and the Natural Science Foundation of Hebei (D2024203001 and 2023HBQZYCSB008; J.L.). B.W. acknowledges Dr. Gaobin Chu for assistance in conducting EPMA measurements and Dr. Zhenyi Zhang for his warm help during the crystal structure refinement. Some experiments were conducted at the Synergetic Extreme Condition User Facility (SECUF proposal No. 2023-SECUF-PT-000570) and BL15U1 at the Shanghai Synchrotron Radiation Facility (SSRF proposal No. 2022-SSRF-PT-020886).

## Author contributions

B.W. and J.L. initiate the project. B.W., J.L., Y.Z., B.N., W.Y., J.H., X.D., and Y.T. perform experiments, data analysis, and interpretation. All authors contribute to the writing and editing of the manuscript.

## Competing interests

The authors declare no competing interests.

## Additional information

**Supplementary information** The online version contains supplementary material available at https://doi.org/10.1038/s41467-025-56312-z.

**Correspondence** and requests for materials should be addressed to Jin Liu.

**Peer review information** *Nature Communications* thanks Geeth Manthilake, and the other, anonymous, reviewer for their contribution to the peer review of this work. A peer review file is available.